

Structure–Conductivity Relationship for Peptoid-Based PEO–Mimetic Polymer Electrolytes

Jing Sun,[†] Gregory M. Stone,^{‡,§} Nitash P. Balsara,^{‡,§,⊥} and Ronald N. Zuckermann^{*,†,§}

[†]Molecular Foundry, Lawrence Berkeley National Laboratory, Berkeley, California 94720, United States

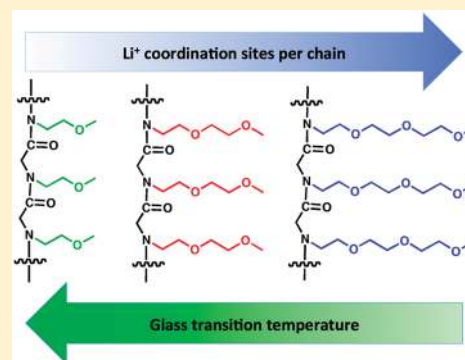
[‡]Department of Chemical and Biomolecular Engineering, University of California, Berkeley, Berkeley, California 94720, United States

[§]Materials Sciences Division, Lawrence Berkeley National Laboratory, Berkeley, California 94720, United States

[⊥]Environmental Energy Technologies Division, Lawrence Berkeley National Laboratory, Berkeley, California 94720, United States

S Supporting Information

ABSTRACT: Polymer electrolytes offer great potential for application in lithium batteries. In order to systematically optimize the performance of these materials, atomic level synthetic control over the polymer chemical structure is desired. In this study, we designed a series of chemically defined, monodisperse peptoid polymers to explore the impact of side-chain structure on the thermal and electrical properties. A series of comblike peptoid homopolymers with ethylene oxide (EO)_n side chains of varying length were synthesized by a rapid solid phase synthetic method. The electrical properties of these materials with dissolved lithium salt were characterized by ac impedance. The temperature dependence of the ionic conductivity of the polypeptoid electrolytes is consistent with the Vogel–Tamman–Fulcher equation. The optimum ionic conductivity of 2.6×10^{-4} S/cm achieved for oligo-*N*-2-(2-(2-methoxyethoxy)-ethoxy)ethylglycine–Li salt complex at 100 °C, is approximately 10-fold lower than the analogous PEO–salt complex. It is, however, nearly 2 orders of magnitude higher than previously reported comblike PEO–mimetic polypeptides. The ionic conductivities of these side chain analogs vary by 3 orders of magnitude, but this variation is entirely governed by the proximity of the system to the glass transition temperature. This investigation shows that polypeptoids provide a unique platform for examining the structure–property relationships of solid polymer electrolytes.



INTRODUCTION

All-solid rechargeable batteries containing a dry polymer electrolyte are promising due to potential of creating systems with high energy densities and extended cycle life. Poly(ethylene oxide) (PEO)-based materials have received the most interest for polymer electrolyte applications due to their high ionic conductivity (around 10^{-3} S/cm at 80 °C).^{1–4} In these electrolytes, the lithium cations are complexed to ether oxygens of the polymer. Thus, the cations are surrounded by a solvation shell as is often the case for cations dispersed in conventional low molecular weight electrolytes, such as water and alkyl carbonates.^{5–7} There are two general mechanisms for ion transport in electrolytes: the ion hopping mechanism wherein ions hop from one liquidlike region to the next, and the vehicular mechanism wherein the ion migrates with the solvation shell more-or-less intact.^{8,9} In polymer electrolytes, the vehicular motion is severely suppressed because motion of the solvation shell requires motion of all of the entangled chains. Ion transport in high molecular weight polymer electrolytes is thus facilitated by rapid segmental motion in the vicinity of the ions. Since polymer segmental motion is affected by the glass transition temperature (T_g), rapid ion transport is generally obtained in low- T_g polymers.

A variety of functional groups other than the ether group can, in principle, be used to solvate lithium cations. The electrolytes in current lithium-ion batteries are mixtures of alkyl carbonates. Nitrogen-containing groups such as nitriles have also been shown to solvate lithium ions.^{10,11} Motivated by these observations, we have designed a family of comblike PEO–mimetic polymers based on an *N*-substituted glycine or peptoid backbone. These polymers contain main-chain tertiary amide functional groups in addition to the side-chain ether oxygens. Polypeptoids are a class of sequence-specific polymer in which chemically diverse side chains are attached to the amide nitrogen.¹² The iterative solid phase submonomer synthesis method allows for the efficient synthesis of polypeptoids of exact monomer sequence from an extremely diverse set of side-chain functionalities derived from readily obtainable reagents.^{13–15} Unlike the typical polyamides, polypeptoids are considerably more flexible due to the lack of backbone hydrogen bonding. This is crucial for solid polymer electrolyte design due to the requirement of rapid segmental motion for ion transport. Hydrogen bonding in polypeptides, nylons, and

Received: April 16, 2012

Revised: May 21, 2012

Published: June 8, 2012

aramides typically dominates the physical properties of the polymers, stabilizing the crystals and raising the melting point. The N-substitution in peptoid polymers eliminates the presence of hydrogen bond donors along the backbone, allowing for a flexible backbone with reduced interchain interactions and excellent thermal processability.¹⁶ Therefore, the crystallization behavior of the polypeptoids is dominated by their side chains. In contrast, PEO is a semicrystalline polymer, and the conductivity of PEO/salt mixtures below 60 °C, the melting point of PEO,¹⁷ decreases as an increasing fraction of the chains are incorporated into the crystals.

Previous studies have addressed the efficacy of polymer electrolytes that contain ether oxygens and other functional groups. Poly[L-methoxytri(ethylene oxide)-L-glutamate] complexes with a variety of alkali metal salts. However, due to the rigid backbone of polypeptides, the ionic conductivity was lower than 10⁻⁵ S/cm at 100 °C.¹⁸ Nagaoka et al. synthesized a linear copolymer with dimethylsiloxane and ethylene oxide segments.¹⁹ A variety of (EO)_n-containing comb-branched copolymers based on polysiloxane²⁰ and polyphosphazene²¹ have been synthesized. None of these studies have demonstrated conductivities comparable to that of PEO-based electrolytes. The main difference between these studies and our work is our ability to exert precise control over monomer and polymer structure and thus to dissect the contribution of various factors on the polymer properties. All of the polymer chains examined in this study contain exactly 20 monomers, and the number of pendant (EO)_n units in the monomers is precisely controlled (*n* = 1–3). This allows us to systematically explore the impact of increasing the number of Li⁺ coordination sites per chain.

PEO-mimetic materials have been widely investigated and used for a variety of applications. In addition to a potential solid polymer electrolyte candidate, peptoids of this class have also been used as mimetics of poly(ethylene glycol) in biological applications. For example, monodispersed homopolymers of *N*-(2-methoxyethyl)glycine (Nmeg) have been used to enhance the solubility of therapeutic peptides for drug delivery²² and to inhibit the fouling of surfaces by the adsorption of proteins.^{23,24} Although quite effective, the only attempt to optimize the chemical structure of these materials was by varying the degree of polymerization. Variety and tunability of side chains enable the systematic study of the relationship between polymer structure and activity and to optimize PEO-mimetic materials based on polypeptoids.

EXPERIMENTAL PART

Synthesis of Submonomers. *Synthesis of 2-(2-Methoxyethoxy)ethyl Tosylate.* In a round-bottom flask, 25 g of diethylene glycol monomethyl ether (0.21 mol) was dissolved in 65 mL of tetrahydrofuran. Upon vigorous stirring at 0 °C, 65 mL of 6 M sodium hydroxide solution was added. To this stirred solution, 50 g of tosyl chloride (0.39 mol) dissolved in 70 mL of THF was added dropwise under N₂. After 1 h, the mixture was allowed to warm to room temperature and then stirred for another hour. Finally, 500 mL of diethyl ether was added, and the organic layer was washed with 1 M aqueous sodium hydroxide and water, sequentially. After drying over MgSO₄, the organic layer was evaporated to yield a colorless liquid (55.5 g). Yield: 96%. ¹H NMR (500 MHz, CDCl₃): δ 7.73 (d, 2H, S-C=CH-CH), 7.27 (d, 2H, S-C=CH-CH), 4.11 (t, 2H, CH₂-CH₂-O-Ts), 3.62 (t, 2H, CH₂-CH₂-O-Ts), 3.51 (m, 2H, CH₃-O-CH₂-CH₂-O), 3.40 (m, 2H, CH₃-O-CH₂-CH₂-O), 3.24 (s, 3H, O-CH₃), 2.37 (s, 3H, C-CH₃).

2-(2-(2-Methoxyethoxy)ethoxy)ethyl tosylate was synthesized with the same protocol. Yield: 96.7%. ¹H NMR (500 MHz, CDCl₃): δ 7.80

(d, 2H, S-C=CH-CH), 7.36 (d, 2H, S-C=CH-CH), 4.14 (t, 2H, CH₂-CH₂-O-Ts), 3.69 (t, 2H, CH₂-CH₂-O-Ts), 3.60 (m, 6H, CH₃-O-CH₂-CH₂-O-(CH₂)₂), 3.52 (m, 2H, CH₃-O-CH₂-CH₂-O), 3.39 (s, 3H, O-CH₃), 2.47 (s, 3H, C-CH₃).

Synthesis of 2-(2-Methoxyethoxy)ethyl Azide. 50 g of 2-(2-methoxyethoxy)ethyl tosylate (0.18 mol) was added to 300 mL of DMF under N₂. Subsequently, 40 g of sodium azide (0.62 mol) was added into the mixture, and the reaction was stirred at 60 °C. After 36 h, the mixture was diluted with a large amount of water and extracted with diethyl ether. The organic layer was washed with water, dried over MgSO₄, and evaporated under vacuum. Yield: 23.0 g, 90%. ¹H NMR (500 MHz, CDCl₃): δ 3.69 (m, 4H, (CH₂)₂O), 3.57 (m, 2H, CH₂-CH₂-N₃), 3.41 (m, 5H, CH₃-O and CH₂-N₃).

2-(2-(2-Methoxyethoxy)ethoxy)ethyl azide was synthesized with the same protocol. Yield: 86%. ¹H NMR (500 MHz, CDCl₃): δ 3.68 (m, 8H, (CH₂)₂O), 3.56 (m, 2H, CH₂-CH₂-N₃), 3.41 (m, 5H, CH₃-O and CH₂-N₃).

Synthesis of 2-(2-Methoxyethoxy)ethylamine. 20 g of 2-(2-methoxyethoxy)ethyl azide (0.14 mol) was dissolved in 160 mL of tetrahydrofuran. Triphenylphosphine (40 g, 0.15 mol) was added, and the reaction was stirred overnight under an atmosphere of nitrogen. The reaction was quenched with 220 mL of water, and the mixture was allowed to stir overnight. The solids were removed by filtration, and the supernatant was washed with toluene and dichloromethane. After concentration in vacuo, 11.8 g of free amine was obtained. Yield: 72%. ¹H NMR (500 MHz, CDCl₃): δ 3.62–3.51 (m, 6H, (CH₂)₂O and CH₂-CH₂-NH₂), 3.37 (s, 3H, CH₃-O), 2.89 (m, 2H, CH₂-CH₂-NH₂).

2-(2-(2-Methoxyethoxy)ethoxy)ethylamine was synthesized with the same protocol. Yield: 84%. ¹H NMR (500 MHz, CDCl₃): δ 3.66–3.50 (m, 10H, (CH₂)₂O and CH₂-CH₂-NH₂), 3.39 (s, 3H, CH₃-O), 2.85 (m, 2H, CH₂-CH₂-NH₂).

Synthesis of Peptoid Polymers. Polypeptoids were synthesized on an automated robotic synthesizer or a commercial Aaptec Apex 396 robotic synthesizer on 100 mg of Rink amide polystyrene resin (0.61 mmol/g, Novabiochem, San Diego, CA). All solvents, and reagents described here were purchased from commercial sources and used without further purification. The synthesis procedure was a modified version of methods previously described.²⁵ The Fmoc group on the resin was deprotected with 20% (v/v) 4-methylpiperidine/DMF before starting the submonomer cycle. An acylation step was then performed on the amino resin by the addition of 1.0 mL of 1.2 M bromoacetic acid in DMF and 0.18 mL of *N,N'*-diisopropylcarbodiimide and mixing for 20 min. Displacement of the bromide with various submonomers occurred by adding a 1.0–2.0 M solution of the primary amine in *N*-methyl-2-pyrrolidone, followed by agitation for 90 min. *N*-(2-Methoxyethyl)glycine polymers (pNme) were acetylated on the resin after synthesis using a mixture (2.0 mL per 100 mg of resin) of 0.4 M acetic anhydride and 0.4 M pyridine in DMF for 30 min. The crude peptoid products were cleaved from the resin by the addition of 50% (v/v) trifluoroacetic acid (TFA) in DCM for 5 min, followed by evaporation under a stream of N₂. Oligo-*N*-2-(2-methoxyethoxy)ethylglycine (pNde) and oligo-*N*-2-(2-methoxyethoxy)ethoxyethylglycine (pNte) were cleaved with 95% (v/v) TFA in water for 5 min before acylation. Subsequently, the mixture was precipitated with an excess of cold diethyl ether under vigorous stirring, followed by centrifugation. The crude cleaved peptoids were then acetylated by the addition of 40 mM of acetic anhydride and 40 mM pyridine in DCM. After 20 min, the reaction mixture was precipitated with an excess of diethyl ether.

The crude products were then dissolved in 1:1 mixture (v/v) of acetonitrile/water and lyophilized. The peptoids were then purified by reverse-phase HPLC on a C18 column (Vydac, 10 μm, 22 mm × 250 mm) using a linear gradient of 5–95% acetonitrile in water with 0.1% TFA over 60 min at a flow rate of 10 mL/min.

Each final product was characterized by analytical reverse-phase HPLC using a C18 column (10 μm, 50 mm × 2 mm) with 5–95% gradient at 1 mL/min over 30 min at 60 °C. Peptoid purity was determined using the analytical reverse-phase HPLC conditions detailed above, and the molecular weight was determined by matrix-

assisted laser desorption/ionization mass spectrometry (Applied Biosystems MALDI TOF/TOF Analyzer 4800) with a 1:1 (v/v) mixture of peptoid (2 mg/mL in 1:1 acetonitrile: water) and 1,8,9-dianthracenetriol dissolved in tetrahydrofuran at 10 mg/mL. The final polypeptoids were then lyophilized prior to subsequent measurements.

Conductivity Measurements. LiTFSI (Li[N(SO₂CF₃)₂, lithium bis(trifluoromethanesulfonyl)imide]) salt from Sigma-Aldrich, was heated at 120 °C under vacuum for 1–2 days to get rid of residual moisture and then stored in an argon-filled glovebox. Polymer electrolytes were prepared by mixing the polypeptoids with an appropriate amount of the LiTFSI salt in the glovebox under an argon atmosphere. The amount of dissolved salt in the polypeptoids is quantified by the molar ratio of cations to peptoid ethylene oxide moieties, r , which ranged from 0.02 to 0.12 in this study. After lyophilization, the mixtures were dried under vacuum at 100 °C for 2–3 days in the antechamber of the glovebox to remove any trace water from the atmosphere. All procedures, performed after this step, were conducted inside the argon-filled glovebox. The polypeptoid electrolytes were loaded into the center of Garolite G-10 spacers with 0.125 mm thickness and a central hole with a diameter of 3.86 mm. A bubble-free disk ~150 μ m thick was obtained in a heated hand press (100 °C) after 5 min. Stainless steel electrodes were placed on both sides of the polypeptoid electrolyte disk to create the electrochemical cell. After measuring sample thickness with a micrometer, the electrochemical cell assembly was placed inside a Swagelok cell holder and connected to a Biologic VMP3 for impedance analysis. The Swagelok cell holder was loaded into a home-built heating chamber. The imaginary and real components of the impedance response, Z' and Z'' , were measured at 10 °C intervals during heating and cooling scans between 30 and 100 °C. An ac signal with a peak voltage of 50 mV was applied in the frequency range (ω) of 10 Hz–1 MHz. An equivalent circuit comprised of a constant phase element in parallel with a resistor was used to calculate the electrolyte resistance from the impedance data. The thickness was measured again after the conductivity measurement.

Differential Scanning Calorimetry (DSC). Differential scanning calorimetry (DSC) experiments were performed to determine the glass transition temperatures of the synthesized peptoids using a TA Q200 differential scanning calorimeter. In all tests, a scan rate of 10 K/min was used in the temperature range of –80 to 200 °C for three heating and cooling cycles.

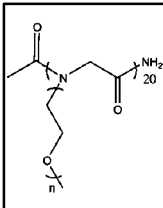
X-ray Diffraction (XRD). X-ray diffraction (XRD) was performed at beamline 8.3.1 at the Advanced Light Source located at Lawrence Berkeley National Laboratory. Samples were thermally annealed in a vacuum oven at 100 °C for 2–3 days before the measurement. ~1 mg of the sample was loaded onto a nylon loop. The signal was radially integrated to obtain a 1D plot of intensity versus scattering angle.

Thermogravimetric Analysis (TGA). Samples were characterized using a TA Instruments TGA to investigate degradation temperatures by mass loss. Approximately 5.0 mg of lyophilized peptoid powder was placed on an aluminum sample pan. Samples were equilibrated at 30 °C for 20 min and then heated to 500 °C at 5 °C/min under a nitrogen atmosphere.

RESULTS AND DISCUSSION

In this article, we designed and synthesized a series of well-defined homopeptoids with a controlled numbers of ethylene oxide units on each side chain. The structure of the synthesized polypeptoids is shown in Table 1 along with their abbreviations. Their molecular weight and purity characteristics are given in Table 1. Their absolute monodispersity was confirmed by analytical HPLC and MALDI mass spectrometry (see Supporting Information, Figure S2). We designed 20mers for the investigation with molecular weights ranging from 2362 to 4128 g/mol. Teran et al. have shown that the ionic conductivity of PEO/LiTFSI mixtures is independent of PEO molecular weight when it exceeds 2000 g/mol.²⁶ It has been previously reported that a wide variety of homopolypeptoids are thermally

Table 1. Model Acetylated Peptoid 20mers and Analytical Data^a

|  | Peptoids (n) | Theoretical molecular weight | Observed molecular weight | Purity of 20-mer (%) |
|--|--------------|------------------------------|---------------------------|----------------------|
| | 1 | 2361.7 | 2362.5 | 90 |
| | 2 | 3242.7 | 3242.8 | 85 |
| | 3 | 4123.9 | 4127.7 | 85 |

^a $n = 1$, Nme = *N*-(2-methoxyethyl)glycine; $n = 2$, Nde = *N*-(2-(2-methoxyethoxy)ethyl)glycine; $n = 3$, Nte = *N*-(2-(2-(2-methoxyethoxy)ethoxy)ethyl)glycine.

stable and their thermal behavior (e.g., glass transition temperature, melting point) are highly tunable and dependent on the monomer structure and sequence.¹⁶ The homopolypeptoids studied here show similar thermal stability, resisting temperatures approaching 300 °C (Figure S2).

DSC traces of all three peptoids are shown in Figure S3. The lack of melting peak and crystallization exotherm indicates that these PEO-mimetic peptoids are noncrystalline. Furthermore, the absence of ordered peaks in the XRD patterns is consistent with the lack of crystalline domain (Figure S4). The glass transition temperatures (T_g) as determined by DSC are shown in Table 2. In general, the T_g values of the polypeptoids

Table 2. T_g of Polypeptoids with and without Salt

| peptoid | T_g (°C) | | |
|--------------------------|----------------------|----------------------|----------------------|
| | p(Nme) ₂₀ | p(Nde) ₂₀ | p(Nte) ₂₀ |
| $r(\text{Li:O}) = 0$ | 38.6 | –6.8 | –26.4 |
| $r(\text{Li:O}) = 0.085$ | 52.2 | 9.9 | –2.4 |

decrease with increasing side-chain EO unit length. Compared to the T_g (38.6 °C) of p(Nme)₂₀, which is above room temperature, p(Nde)₂₀ and p(Nte)₂₀ have significantly lower T_g s, around –6.8 and –26.4 °C, respectively. These values are higher than the T_g of neat PEO ($M_n = 2000$), reported to lie between –30 and –60 °C. It is noted that the T_g of PEO depends on the fraction of crystalline domains.^{27,28} There is a large T_g gap between polypeptoids with one and two EO residues in the side chain [p(Nme)₂₀ vs p(Nde)₂₀], though the weight fraction of EO moieties in the neat polypeptoids increases gradually from 50.0% to 63.6% and 71.4% with the increasing size of the side chain. It is clear that segmental motion, which is directly related to T_g , depends not only on the composition of the monomer but also on the arrangement of the rapidly moving segments, (EO)_{*n*}.

As shown in Table 2, the complexation of the polypeptoid with lithium salts raises the glass transition temperature for all of these polypeptoids. Furthermore, the T_g increases linearly with increasing salt concentration, r (Figure 1). This is not unexpected, as polymer chains coordinate with lithium ions to form ionic cross-links,²⁹ which limit the mobility of the polymer chains, resulting in a higher T_g . More interestingly, the slope of the T_g versus r line is larger for p(Nte)₂₀ than for p(Nde)₂₀ and p(Nme)₂₀. It is evident that the impact of lithium salt on the peptoid T_g is greater for p(Nte)₂₀ than for p(Nde)₂₀ and p(Nme)₂₀. For r values greater than 0.15, the T_g of the complex based on p(Nte)₂₀ is higher than the one based on p(Nde)₂₀. Similar behavior has been observed in (EO)_{*n*}-containing comblike polystyrene.³⁰ Molecular dynamics simulations³¹

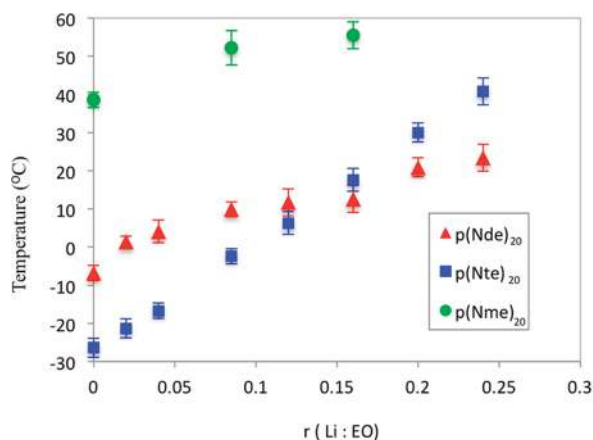


Figure 1. T_g of the polymer electrolytes versus salt concentration r .

and neutron diffraction data³² indicate that the Li^+ ions are coordinated with PEO through five ether oxygens of a polymer chain.³³ p(Nte)_{20} has longer side chains that appear to be more effective in coordinating Li^+ . We thus expect the segmental motion at a fixed temperature to be more rapid in p(Nte)_{20} in the $0 < r < 0.15$ regime. In the $0.15 < r < 0.24$ regime we expect more rapid segmental motion in p(Nde)_{20} at the same temperature. The question of how changes in the strength of complexation and segmental motion affect conductivity is an interesting question that we will address shortly.

The ionic conductivities of several polypeptoid/LiTFSI polymer electrolytes were measured as a function of temperature and salt concentration. Measured values of ionic conductivity of the three polymer electrolyte systems [p(Nme)_{20} , p(Nde)_{20} , and p(Nte)_{20}] at $r = 0.085$, at temperatures between 30 and 100 °C, are shown in Figure 2. In each case the

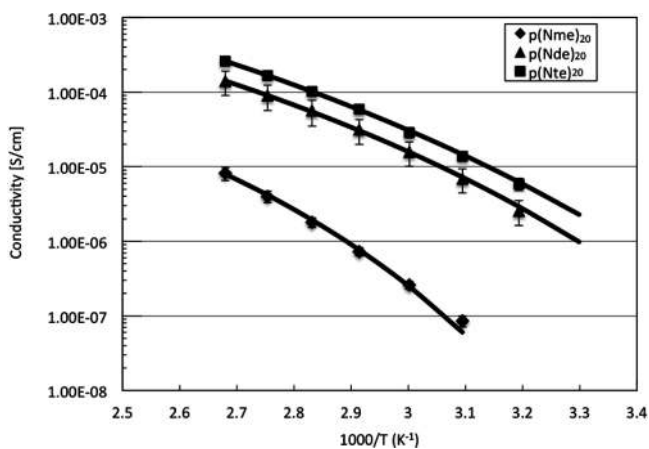


Figure 2. Ionic conductivity plots as a function of temperature at a salt concentration of $r = 0.085$. The lines through the data points are VTF fits.

ionic conductivity increases with increasing temperature, as is typical of polymer electrolytes. The Vogel–Tamman–Fulcher (VTF) equation,³⁴ which is typically used to describe the steep dependence of viscosity on temperature in the vicinity of the glass transition, is often used to describe the temperature-dependent conductivity data of polymer electrolytes.

$$\sigma(T) = A \exp\{-B/(R(T - T_0))\}$$

In this expression, σ is the ionic conductivity, A is a constant proportional to the number of charge carriers, B is equivalent to the activation energy for ion motion, R is the gas constant, T is the temperature, and T_0 is a reference temperature, which is $T_g(r, n) - 83$ K; note that the T_g of the electrolytes depends on both salt concentration and length of the side chains. Unlike linear PEO, the PEO–mimetic polypeptoids do not crystallize in our temperature window (regardless of salt concentration), and thus the VFT equation fits the entire data set in Figure 2. The polypeptoid with the largest molecular weight shows the highest conductivity; it should be clear that the conductivity of our electrolytes is dominated by segmental motion, not vehicular motion. The conductivity of p(Nde)_{20} and p(Nte)_{20} is significantly higher than that of p(Nme)_{20} . We thus focus on p(Nde)_{20} and p(Nte)_{20} in our discussion of the effect of salt concentration.

Ionic conductivity of PEO–mimetic polypeptoids varies significantly with the concentration of lithium salt dissolved in the polymer, shown as in Figure 3. With increasing salt

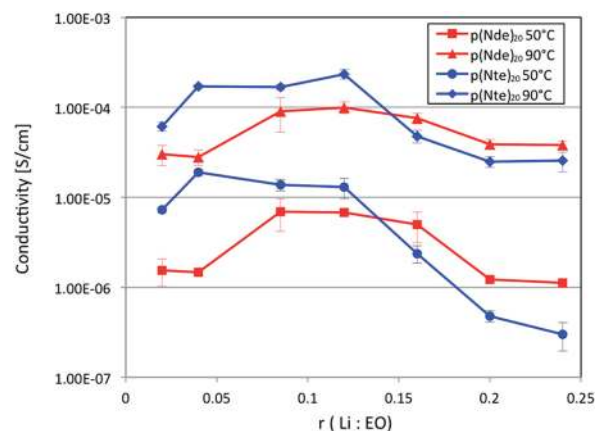


Figure 3. Ionic conductivity plots as a function of salt concentration r at 50 and 90 °C.

concentration, the conductivity of the electrolytes initially increases because more charge carriers are incorporated into the system, despite a modest rise in T_g . However, as the salt concentration increases further, the ionic conductivities in both systems levels off and eventually decreases. This behavior can be explained by considering the opposing influences of chain mobility (as measured by the T_g) and charge carrier density (proportional to salt concentration). For the p(Nte)_{20} –Li salt complexes, the T_g increases rapidly with increasing temperature (Figure 1). The increasing concentration of charge carriers results in an increase in conductivity at low r values, but this is eventually offset by the decrease in segmental motion, resulting at high r values. This eventually results in lower conductivities at $r > 0.14$. Qualitatively similar behavior is seen in the p(Nde)_{20} –Li salt complexes. In general, the ionic conductivities of the p(Nte)_{20} –salt complexes are higher than those of the p(Nde)_{20} complexes, until $r(\text{Li:O})$ reaches 0.14. Interestingly, a crossover in conductivity between p(Nte)_{20} and p(Nde)_{20} takes place at an r of 0.14, which is approximately the same point at which their T_g 's cross over (Figure 1). The p(Nde)_{20} electrolyte conductivity at the highest r values is comparable to that at low r values at both 50 and 90 °C. In contrast, the p(Nte)_{20} electrolyte conductivity at the highest r values is significantly lower than that at low r values at 50 °C.

The relative importance of complexation and segmental motion of conductivity is addressed in Figure 4 where the

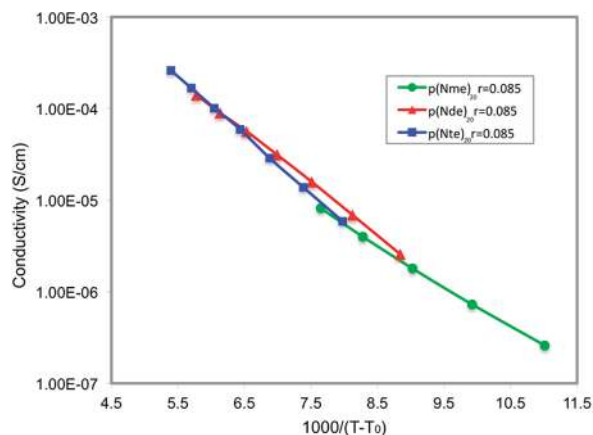


Figure 4. Ionic conductivity plots as a function of $1000/(T - T_0)$ where $T_0 = T_g - 83$ K. Note that T_g depends on both salt concentration (r) and side chain length (n).

conductivity of all 3 polymers at $r = 0.085$ is plotted versus $1/(T - T_g(r, n) - 83$ K) on a semilog scale. All of the data collapse on to a single line. A fit through the data yields

$$\sigma(T) = 0.485 \exp\{-1400/(T - T_0)\}$$

The collapse in Figure 4 indicates that the conductivity of all of the electrolytes is dominated by segmental motion, not by complexation. The large changes in monomer structure as n is varied from 1 to 3 have no impact on ion transport other than the effect of this on segmental motion. This suggests that the introduction of amide linkages in the polypeptoid backbone do not significantly affect the coordination between the polymer and the ions (Li^+ and TFSI^-). Thus, the poor conductivity of p(Nme)_{20} seen in Figure 2 is attributed entirely due to the slow segmental motion and not the inability of the single pendant EO unit to coordinate with Li^+ . Similarly, the interesting crossover in conductivities of p(Nde)_{20} and p(Nte)_{20} seen in Figure 3 is also entirely due to changes in segmental motion. Plotting all the other ionic conductivities with different r and n as a function of $1000/(T - T_0)$ showing the same slope (Figure S5) confirms this conclusion. These data lie on different curves because the number of charge carriers related to A is changing with different r , but irrespective of n (Table S2).

CONCLUSION

Three new comblike PEO-mimetic polypeptoids of absolute monodispersity and varying side chain length have been designed and synthesized by a solid phase synthetic method. Their thermodynamic properties and ionic conductivity of dry polymer electrolytes made by mixing the polypeptoids with LiTFSI have been explored. The polypeptoids with longer EO side chains materials are excellent PEO-mimetic materials that exhibit rapid segmental motion and are capable of complexing lithium ions. The maximum conductivity of 2.6×10^{-4} S/cm in the p(Nte)_{20} complex ($r = 0.085$) at 100°C is ~ 2 orders of magnitude higher than PEO-mimetic polypeptides¹⁸ but significantly lower than that of PEO homopolymers at the same salt concentration. The ability to fine-tune the intra- and intermolecular interactions in a simple way makes the peptoid system an excellent choice to examine the relationship between

the ionic conductivity and the chemical structure of the polymer electrolytes. In particular, we showed that the large changes in conductivity seen in the systems at a fixed temperature and salt concentration were correlated to changes in T_g and not changes in other factors such as complexation and length of the pendant $(\text{EO})_n$ chains. Although, it is worth mentioning that the T_g can be dependent on the strength of complexation and length of pendant side chains. We hope that such systematic studies will enable the design of polymer electrolytes with higher conductivity than PEO and the incorporation of other functional groups that can help rapid transport of the lithium ions. Furthermore, the incorporation of the homopolypeptoid blocks into a diblock copolymer with a mechanically robust block is likely to yield polymer electrolyte materials with high conductivity and high modulus.³⁵ The precise tunability of polypeptoids offer a platform for the fundamental study of the structure-conductivity relationship of block polymer electrolytes in a facile way.

ASSOCIATED CONTENT

Supporting Information

¹H NMR spectra of the submonomers, analytical HPLC and MALDI spectra, differential scanning calorimetry data, TGA, XRD for polypeptoids. This material is available free of charge via the Internet at <http://pubs.acs.org>.

AUTHOR INFORMATION

Corresponding Author

*E-mail: rnzuckermann@lbl.gov.

Notes

The authors declare no competing financial interest.

ACKNOWLEDGMENTS

Funding for this work was provided by the Soft Matter Electron Microscopy Program, supported by the Office of Science, Office of Basic Energy Science, U.S. Department of Energy, under Contract DE-AC02-05CH11231. The work was carried out at the Molecular Foundry at Lawrence Berkeley National Laboratory, supported by the Office of Science, Office of Basic Energy Science, U.S. Department of Energy, under Contract DE-AC02-05CH11231. We thank Dr. Daniel Hallinan, Scott Mullin, and Alexander Teran for helpful advice and Babak Sanii for help with the XRD experiments.

REFERENCES

- (1) Fenton, D. E.; Parker, J. M.; Wright, P. V. *Polymer* **1973**, *14*, 589.
- (2) Christie, A. M.; Lilley, S. J.; Staunton, E.; Andreev, Y. G.; Bruce, P. G. *Nature* **2005**, *433*, 50.
- (3) Gray, F. M. *Solid Polymer Electrolytes: Fundamentals and Technological Applications*, Wiley-VCH: New York, 1991.
- (4) Berthier, C.; Gorecki, W.; Minier, M.; Armand, M. B.; Chabagno, J. M.; Rigaud, P. *Solid State Ionics* **1983**, *11*, 91.
- (5) Borodin, O.; Smith, G. D. *J. Solution Chem.* **2007**, *36*, 803.
- (6) Druger, S. D.; Nitzan, A.; Ratner, M. A. *J. Chem. Phys.* **1983**, *79*, 3133.
- (7) Nitzan, A.; Ratner, M. A. *J. Phys. Chem.* **1994**, *98*, 1765.
- (8) Diddens, D.; Heuer, A.; Borodin, O. *Macromolecules* **2010**, *43*, 2028.
- (9) Shi, J.; Vincent, C. A. *Solid State Ionics* **1993**, *60*, 11.
- (10) Alarco, P. J.; Abu-Lebdeh, Y.; Abouimrane, A.; Armand, M. *Nat. Mater.* **2004**, *3*, 476.
- (11) Watanabe, H.; Kotaka, T. *Macromolecules* **1984**, *17*, 2316.
- (12) Kirshenbaum, K.; Zuckermann, R. N.; Dill, K. A. *Curr. Opin. Struct. Biol.* **1999**, *9*, 530.

- (13) Simon, R. J.; Kania, R. S.; Zuckermann, R. N.; Huebner, V. D.; Jewell, D. A.; Banville, S.; Ng, S.; Wang, L.; Rosenberg, S.; Marlowe, C. K.; Spellmeyer, D. C.; Tan, R. Y.; Frankel, A. D.; Santi, D. V.; Cohen, F. E.; Bartlett, P. A. *Proc. Natl. Acad. Sci. U. S. A.* **1992**, *89*, 9367.
- (14) Figliozzi, G. M.; Goldsmith, R.; Ng, S. C.; Banville, S. C.; Zuckermann, R. N. *Methods Enzymol.* **1996**, *267*, 437.
- (15) Nam, K. T.; Shelby, S. A.; Choi, P. H.; Marciel, A. B.; Chen, R.; Tan, L.; Chu, T. K.; Mesch, R. A.; Lee, B.-C.; Connolly, M. D.; Kisielowski, C.; Zuckermann, R. N. *Nat. Mater.* **2010**, *9*, 454.
- (16) Rosales, A. M.; Murnen, H. K.; Zuckermann, R. N.; Segalman, R. A. *Macromolecules* **2010**, *43*, 5627.
- (17) Wang, C. X.; Sakai, T.; Watanabe, O.; Hirahara, K.; Nakanishi, T. *J. Electrochem. Soc.* **2003**, *150*, A1166.
- (18) Yamaguchi, Y.; Aoki, S.; Watanabe, M.; Sanui, K.; Ogata, N. *Solid State Ionics* **1990**, *40*, 628.
- (19) Nagaoka, K.; Naruse, H.; Shinohara, I.; Watanabe, M. *J. Polym. Sci., Polym. Lett. Ed.* **1984**, *22*, 659.
- (20) Spinder, R.; Shriver, D. E. *J. Am. Chem. Soc.* **1988**, *10*, 3036.
- (21) Blonsky, P. M.; Shriver, D. F.; Austin, P.; Allcock, H. R. *J. Am. Chem. Soc.* **1984**, *106*, 6854.
- (22) Statz, A. R.; Park, J. P.; Congsiriwatana, N. P.; Barron, A. E.; Messersmith, P. B. *Biofouling* **2008**, *24*, 439.
- (23) Park, M.; Jardetzky, T. S.; Barron, A. E. *Pept. Sci.* **2011**, *96*, 688.
- (24) Statz, A. R.; Meagher, R. J.; Barron, A. E.; Messersmith, P. B. *J. Am. Chem. Soc.* **2005**, *127*, 7972.
- (25) Monroe, C.; Newman, J. J. *Electrochem. Soc.* **2005**, *152*, A396.
- (26) Teran, A. A.; Tang, M. H.; Mullin, S. A.; Balsara, N. P. *Solid State Ionics* **2011**, *203*, 18.
- (27) Back, D. M.; Schmitt, R. L. *Encyclopedia of Polymer Science and Technology*; Wiley-Interscience: New York, 2004; Vol. 9, p 805.
- (28) Faucher, J. A.; Koleske, J. V.; Santee, E. R.; Stratta, J. J.; Wilson, C. W. *J. Appl. Phys.* **1966**, *37*, 3962.
- (29) Allcock, H. R.; Kellam, E. C. *Solid State Ionics* **2003**, *156*, 401.
- (30) Inoue, K.; Nichikawa, Y.; Tanigaki, T. *J. Am. Chem. Soc.* **1991**, *113*, 7609.
- (31) Borodin, O.; Smith, G. D. *Macromolecules* **1998**, *31*, 8396.
- (32) Saboungi, M. L.; Price, D. L.; Mao, G. M.; Perea, R. F.; Borodin, O.; Smith, G. D.; Michel, A.; Howells, W. S. *Solid State Ionics* **2002**, *147*, 225.
- (33) Meyer, W. H. *Adv. Mater.* **1998**, *10*, 439.
- (34) Gray, F. M. *Polymer Electrolytes*; The Royal Society of Chemistry: Cambridge, 1997; p 175.
- (35) Singh, M.; Odusanya, O.; Wilmes, G. M.; Eitouni, H. B.; Gomez, E. D.; Patel, A. J.; Chen, V. L.; Park, M. J.; Fragouli, P.; Iatrou, H.; Hadjichristidis, N.; Cookson, D.; Balsara, N. P. *Macromolecules* **2007**, *40*, 4578.